Impact of high-temperature implantation of Mg ions into GaN

Masahiro Takahashi[1]*, Atsushi Tanaka[2,3], Yuto Ando[1], Hirotaka Watanabe[2], Manato Deki[2], Maki Kushimoto[1], Shugo Nitta[2], Yoshio Honda[2], Kohei Shima[4], Kazunobu Kojima[4], Shigefusa F. Chichibu[2,4], and Hiroshi Amano[2,3,5,6]

[1] *Graduate School of Engineering, Nagoya University, Nagoya 464-8603, Japan*

[2] *Institute of Materials and Systems for Sustainability, Nagoya University, Nagoya 464-8601, Japan*

[3] *National Institute for Materials Science, Tsukuba 305-0044, Japan*

[4] *Institute of Multidisciplinary Research for Advanced Materials, Tohoku University, Sendai 980-8577, Japan*

[5] *Akasaki Research Center, Nagoya University, Nagoya 464-8603, Japan*

[6] *Venture Business Laboratory, Nagoya University, Nagoya 464-8603, Japan*

*E-mail: m_takaha@nuee.nagoya-u.ac.jp

Magnesium (Mg) ion implantation into gallium nitride (GaN) at 1000 °C is proposed. Since ion implantation and annealing occur simultaneously in high-temperature implantation, it is considered that Mg ions can be introduced at an appropriate position upon their implantation. GaN vertical diodes implanted with Mg ions were fabricated and current–voltage measurements were performed. As a result, clear rectifying properties were confirmed in a sample that was implanted with Mg ions at 1000°C and annealed after implantation. However, the sample subjected to Mg ion implantation at RT and annealed after implantation showed no clear rectification. These results show that high-temperature implantation of Mg ions at 1000°C suppresses crystal degradation during the implantation and simultaneously activates Mg ions upon their implantation. Therefore, it is suggested that 1000°C or higher is required to obtain the high-temperature implantation effect by Mg ion implantation into GaN.

1. Introduction

Gallium nitride (GaN) is expected to be used as a material for post-Si semiconductor power devices because it has excellent physical properties such as a high breakdown field and high saturation electron velocity. Ion implantation, which enables local doping at an arbitrary concentration, is an essential process for realizing a vertical GaN power device. When using the ion implantation technique, etching and regrowth are not required, an in-plane p−n junction can be easily fabricated, and the process cost is low. Moreover, the formation of a local n-type or p-type region in metal-oxide-semiconductor field-effect transistor (MOSFET) fabrication and the formation of a guard ring for an electric field relaxation structure at the edge termination are expected to be achieved by the ion implantation technique. In this paper, we propose magnesium (Mg) ion implantation at a high temperature. Since ion implantation and annealing may occur simultaneously during high-temperature implantation, we consider that Mg ions can be introduced at an appropriate position upon their implantation. On the basis of the results of positron annihilation spectroscopy measurement, a high concentration of vacancy-type defects consisting of a gallium vacancy (V_{Ga}) and a nitrogen vacancy (V_N) ($V_{Ga}V_N$) were generated when Mg ion implantation was performed at RT.[1,2] In addition, vacancy-type defects in the samples implanted with a Mg concentration ([Mg]) of 1×10^{18} or 1×10^{19} cm^{-3} have been reported to aggregate into larger vacancy clusters $(V_{Ga})_3(V_N)_3$ when annealed above 1000°C after Mg ion implantation at RT.[1] Since V_Ns are likely to act as donors,[3] suppressing their formation is essential to realizing p-type conductivity. However, it has been reported that if a sample implanted with [Mg] of 1×10^{17} cm^{-3} is annealed at temperatures between 1000 and 1100°C, vacancy aggregation is suppressed.[1] From these reports, we consider the advantages of high-temperature implantation as follows. In case of RT implantation, a large number of vacancy-type defects are introduced due to damage by Mg ion implantation, and it is necessary to recover those defects by post-implantation annealing. During the recovery of these defects, it is considered that vacancy-type defects become larger due to aggregation. However, in case of high-temperature implantation, it is considered that the aggregation of the vacancy-type defects can be suppressed by performing post-implantation annealing in a state where the damage by Mg ion implantation is small, that is, with few vacancy-type defects. On the basis of this idea of high-temperature implantation, we consider that vacancy-type defect

aggregation is less likely to occur during high-temperature implantation of Mg ions into GaN than during post-implantation annealing after high-concentration Mg ion implantation at RT. However, it has been reported that the vacancy-type defects were $V_{Ga}V_N$ in an as-implanted sample implanted at RT,[1,2] but these defects aggregated into $V_{Ga}(V_N)_2$ in an as-implanted sample implanted at 500°C.[4] There are reports on the high-temperature implantation of Mg ions into GaN,[4-10] but a temperature of approximately 500°C is commonly used. According to a paper on the high-temperature implantation of argon (Ar) ions into GaN, the amount of disorder in the bulk region inside the GaN surface induced by Ar ion implantation was investigated by Rutherford backscattering spectroscopy.[11] The amount of disorder up to an implantation temperature of 500°C decreases as the implantation temperature increases.[11] However, the amount of disorder when the implantation temperature is about 500°C to 700°C increases as the implantation temperature increases.[11] The amount of disorder induced by Ar ion implantation shows a behavior reversed by the implantation temperature and is called "reverse annealing".[11] Further, the amount of disorder when the implantation temperature is 800°C or higher decreases as the implantation temperature increases.[11] From these results, to prevent vacancy-type defects from agglomerating and to prevent reverse annealing during high-temperature implantation, it is considered that Mg ions should be implanted at temperatures higher than 800°C, which has been the implantation temperature commonly used. For this reason, it is necessary to investigate an appropriate Mg ion implantation temperature for GaN.

In recent years, Mg ion implantation technology for GaN has been greatly advanced by the use of high-quality free-standing GaN substrates. It has been reported that a p−n junction can be formed by Mg ion implantation, and rectification characteristics and electroluminescence have been observed.[12-14] The operation of latetral MOSFETs using a Mg-ion-implanted layer or vertical MOSFETs using an all ion implantation process has been confirmed.[15-18] In addition, Sakurai et al. reported that the thermal decomposition of GaN can be prevented even at 1480°C by post-implantation annealing in an ultra-high-pressure N_2 atmosphere of 1 GPa.[19] Temperature-dependent Hall-effect measurement has been performed on a Mg-ion-implanted sample subjected to ultra-high-pressure annealing, and the formation of a p-GaN layer was reported.[19] However, this method requires an ultra-high-pressure of 1 GPa, and p-GaN layer formation by Mg ion implantation still has significant

problems in practical use, such as small sample size and high cost. Therefore, it is necessary to study other methods of forming a p-GaN layer by Mg ion implantation. In this paper, we propose high-temperature implantation rather than a special method of post-implantation annealing. In this study, to investigate the effects of implantation temperature on Mg ion implantation into GaN and the usefulness of high-temperature implantation, Mg ion implantation was performed at a high temperature and the samples were evaluated.

2. Experimental methods

An illustration of the simple process flow and sample structure is shown in Fig. 1. The ion-implanted samples were fabricated as follows. About 5 μm of unintentionally doped (UID-) GaN was grown by metal organic vapor phase epitaxy (MOVPE) on a +*c*-plane n-type GaN free-standing substrate. Thereafter, a silicon nitride (SiN) layer with a thickness of 40 nm was formed on both sides of each sample by plasma-enhanced chemical vapor deposition (PECVD). The SiN layer functions as a through film to adjust [Mg] on the GaN surface and reduce damage caused by ion implantation, as well as a protective film against thermal decomposition during implantation at high temperatures. Mg ions at doses of 2.8×10^{13} and 1.3×10^{14} cm^{-2} were implanted into the GaN layer at energies of 40 and 100 keV, respectively. The Mg depth profile estimated by stopping and range of ions in matter (SRIM) simulation is shown in Fig. 2. The [Mg] distribution was designed to have a box-type profile with a concentration of about 1×10^{19} cm^{-3} and a depth of about 100 nm. The implantation angle was set to 7° to suppress channeling. The ion implantation temperatures were RT, 800 °C, and 1000 °C. The ion implantation was performed in a vacuum of about 10^{-4} Pa or less and in an environment in which GaN is likely to be thermally decomposed, so it was difficult to maintain a temperature higher than 1000 °C during ion implantation. The high-temperature implantation was performed by heating with IR irradiation from the back of the sample, and the sample temperature was measured by placing a thermocouple in contact with the sample surface. To separate the high-temperature implantation from the post-implantation annealing, the temperature was maintained only during Mg ion implantation, and heating was stopped when the implantation was completed. The total time maintained at the set temperature during the high-temperature implantation, including the time before the start of implantation and after the end of implantation, was less than 5 min. In this paper, a sample obtained

immediately after Mg ion implantation is called an “as-implanted” sample. After removing the SiN layer with diluted HF, a SiN layer with a thickness of 40 nm was formed again on both sides by PECVD as a protective film for post-implantation annealing. All samples were annealed at 1250 °C for 20 s in N_2 gas at atmospheric pressure. When performing post-implantation annealing, the susceptor temperature was measured with a thermocouple. Therefore, in order to bring the Mg-ion-implanted layer side into contact with the susceptor, the samples were turned upside down as shown in Fig. 1. In this paper, a sample obtained immediately after post-implantation annealing is called an “after annealing” sample. After removing the SiN layer, vertical diodes of Mg-ion-implanted GaN were fabricated. Ni/Au was deposited using an electron beam evaporator to form 300-μm-diameter anodes on the Mg-ion-implanted layer. Sintering annealing was performed in O_2 gas at 525 °C for 5 min. Finally, a bottom ohmic electrode was formed by depositing Al by sputtering.

3. Results and discussion

3.1 Mg-ion-implanted GaN before post-implantation annealing

First, the evaluations were performed on the samples without post-implantation annealing to determine the impact of the high-temperature implantation of Mg ions into GaN. To investigate the damage to the lattice caused by Mg ion implantation, X-ray diffraction (XRD) analysis was performed. Figure 3 shows the XRD spectra in the 2θ–ω scan mode of as-implanted Mg-ion-implanted samples and unimplanted UID-GaN. By 2θ–ω scanning of GaN(0002), we investigated the lattice distortion in the *c*-axis direction. In the RT implantation sample, peaks were observed on the low-angle side of GaN(0002), as indicated by the arrow in Fig. 3. This is because the lattice expanded in the *c*-axis direction owing to the damage caused by Mg ion implantation. It has been reported that the peak corresponding to lattice expansion is observed in samples implanted with not only Mg but also other elements before post-implantation annealing.[7,8,20-22] However, in the samples implanted with Mg ions at high temperatures, no such peaks corresponding to lattice damage were observed, and the crystallinity after Mg ion implantation measured by XRD seemed to approach that of unimplanted UID-GaN. From the XRD 2θ–ω scan results, it is considered that the damage formed at the time of Mg ion implantation can be reduced by implanting Mg ions at a high temperature.

The luminescence characteristics of GaN samples after Mg ion implantation were evaluated by photoluminescence (PL) measurement. Figure 4 shows the PL spectra at 77 K for as-implanted Mg-ion-implanted samples subjected to excitation by a 325 nm He–Cd laser. The excitation intensity of the PL was 30 kW cm^{-2}. The near-band-edge (NBE) emission observed at around 3.47 eV suggests a decrease of the concentration of nonradiative recombination channels by damage induced during Mg ion implantation, and the Mg-related donor−acceptor-pair (DAP) emission observed at around 3.28 eV indicates the activation of Mg. The green luminescence (GL) band with a peak at around 2.35 eV in low-temperature PL measurements is considered to originate from V_Ns.[23,24] According to Reshchikov et al.,[23] the characteristic GL band peak due to V_N is called GL2 to distinguish it from other green bands. The GL band is a characteristic emission observed in Mg-ion-implanted GaN,[7,11,24-26] and is only weakly observed from epitaxially grown Mg-doped p-GaN.[24,27] In the RT implantation sample [Fig. 4(a)], V_{Ga}s and V_Ns are generated as a result of the damage caused by the Mg ion implantation, and since they are considered to act as nonradiative recombination channels, emission was hardly observed.[24] In the 800 °C implantation sample [Fig. 4(b)], the GL band was clearly observed and weak DAP emission was also observed. It was found during heating that Mg began to be activated at 800 °C. The NBE emission, DAP emission, and GL band were clearly observed in the 1000 °C implantation sample [Fig. 4(c)]. Since no NBE emission was observed in the RT implantation sample, the 325 nm line of a He−Cd laser is most likely fully absorbed in the Mg-ion-implanted layer, and no emission from underlying UID-GaN layer would be detected. This result indicates that NBE emission observed in the 1000 °C implantation sample was not from the underlying UID-GaN layer but from the Mg-ion-implanted GaN layer. It is considered that the concentration of the nonradiative recombination channels in the Mg-ion-implanted layer decreased, and NBE emission was observed. The PL spectra suggest that the high-temperature implantation of Mg ions into GaN leads to a decrease of the concentration of nonradiative recombination channels and the activation of Mg simultaneously with the implantation.

Transmission electron microscopy (TEM) analysis was performed to evaluate the disorder of crystals caused by Mg ion implantation. In Mg-ion-implanted GaN, formation of defects such as pyramidal shape, line shape, and elliptical shape in cross-sectional scanning TEM (STEM) has been reported.[9] In addition, it has been reported that Mg aggregates in defect

regions.[28] Since Mg aggregation reduces the concentration of Mg in areas other than the defect regions, it is necessary to suppress the formation of defects. Figure 5 shows cross-sectional TEM images of as-implanted Mg-ion-implanted GaN samples. In the RT implantation sample [Fig. 5 (a)], a change can be seen from the GaN surface to a depth of about 120 nm. The crystallinity deteriorated owing to the damage caused by Mg ion implantation, and dark regions were formed. More serious deterioration of crystallinity seems to occur, especially at 30 nm or less from the surface. In the 800 °C implantation sample [Fig. 5(b)], a large number of circular defects were seen from the GaN surface to a depth of about 160 nm. It seems that these defects were moved and aggregated by heating during Mg ion implantation. In the 1000 °C implantation sample [Fig. 5(c)], many elliptical defects with a length of about 10 nm were observed from the GaN surface to a depth of about 230 nm. Compared with the number of circular defects of the 800 °C implantation sample, the number of elliptical defects of the 1000 °C implantation sample was smaller, and the recovery of crystallinity was observed in regions other than the defects. This result suggests that by performing Mg ion implantation at a high temperature, damage induced by Mg ion implantation can be reduced and the deterioration of crystallinity after Mg ion implantation can be prevented. However, it seems that elliptical defects were formed because the atoms can move easily at a high temperature. The recovery of the crystallinity of the 1000 °C implantation sample is supported by the observation of NBE emission in the PL measurement.

In the as-implanted GaN implanted with Mg ions at 1000 °C, no peak corresponding to lattice damage was observed in the XRD 2θ–ω scan. NBE emission, suggesting a decrease of the concentration of nonradiative recombination channels by damage induced during Mg ion implantation, and DAP emission, indicating the activation of Mg, were observed in the results of low-temperature PL measurement. Moreover, regions where the crystallinity recovered were observed in the cross-sectional TEM image. These results show that high-temperature implantation of Mg ions into GaN at 1000 °C reduces damage induced during Mg ion implantation and can simultaneously activate Mg ions upon their implantation.

3.2 Mg-ion-implanted GaN after post-implantation annealing

Next, post-implantation annealing was performed. The impact of the temperature during Mg

ion implantation after post-implantation annealing was investigated by low-temperature PL and cross-sectional TEM, similarly to the as-implanted sample.

Figure 6 shows the PL spectra at 77 K for Mg-ion-implanted samples after annealing. In the samples after annealing, the NBE and DAP emission, their LO phonon replicas, and the GL band were observed in all samples. In comparison with the results of the as-implanted samples shown in Fig. 4, the intensity of NBE and DAP emission increased in the RT and 800 °C implantation samples that performed post-implantation annealing. This result suggests that post-implantation annealing reduced the concentration of nonradiative recombination channels and activated Mg in RT and 800 °C implantation samples. On the other hand, in the 1000 °C implantation sample, the intensity of NBE emission did not substantially change and the intensity of DAP emission decreased in the post-implantation annealing sample, as compared with the as-implanted sample. V_{Ga} complexes with V_Ns are reported to act as nonradiative recombination channels.[24] Therefore, it is considered that N out-diffusion from the GaN surface occurred during the post-implantation annealing, and the concentration of nonradiative recombination channels may have increased due to the increased V_N concentration. From these results, we consider as follows. It is considered that V_Ns increase also occurred in the RT and 800 °C implantation samples due to N out-diffusion from GaN surface during post-implantation annealing. However, it is considered that the decrease due to post-implantation annealing of V_Ns introduced by the Mg ion implantation damage contributed, and the intensity of NBE and DAP emission increased. On the other hand, in the as-implanted 1000 °C implantation sample, the amount of V_Ns introduced by Mg ion implantation damage may be smaller than that in the RT and 800 °C implantation samples due to high-temperature implantation. Therefore, it is considered that the increase in V_Ns due to N out-diffusion from GaN surface during the post-implantation annealing greatly contributed, and the intensity of DAP emission was reduced. The PL spectra of the GL band showed almost no change in GL intensity, which was luminescence due to V_Ns,[23,24] in each sample after annealing. However, as shown on a linear scale in Fig. 6(d), the intensity of DAP emission increased as the implantation temperature increased, and that the intensity of NBE emission increased with high-temperature (800 and 1000 °C) implantation compared to RT implantation. Therefore, these results suggest that the concentration of nonradiative recombination channels was decreased by the high-temperature implantation.

Figure 7 shows cross-sectional TEM images of Mg-ion-implanted GaN samples after annealing. In the RT implantation sample [Fig. 7(a)], small circular defects were seen from the GaN surface to a depth of about 130 nm. In the 800 °C implantation sample [Fig. 7(b)], defects were seen from the GaN surface to about 150 nm in depth the shape of which was similar to that of the defects in the RT implantation sample after annealing [Fig. 7(a)]. In the 1000 °C implantation sample [Fig. 7(c)], elliptical defects were observed from the GaN surface to about 200 nm in depth the shape of which was similar to that of the defects in the as-implanted 1000 °C implantation sample [Fig. 5(c)]. In Ref. [28], cross-sectional low angle annular dark field-STEM images of Mg-ion-implanted GaN that was annealed at 1000 to 1300 °C are reported, and it is reported that the number of defects decreased as the annealing temperature increased. Also, it can be seen that the defect size has increased with the increase in the annealing temperature. For this reason, it is considered that the number and size of lattice distortion due to defects are determined by the thermal history of the sample. In the comparison of the after annealing samples, similar defects were observed in the RT and 800 °C implantation samples, and the different defects were observed at 1000 °C implantation. It is considered that the TEM images of after annealing samples as follows. Since the post-implantation annealing was performed at 1250 °C which is greatly higher than implantation temperature, it is believed that the thermal history of the post-implantation annealing contributed to defect generation at implantation temperatures up to 800 °C. For this reason, it is considered that a similar defect occurred in the RT and 800 °C implantation samples. On the other hand, for 1000 °C implantation sample, defects generated by heating during ion implantation did not showed size change due to post-implantation annealing at 1250 °C. This phenomenon is thought to be due to the thermal history during ion implantation that contributed to the generation of defects. In addition, the results of the 1000 °C implantation sample suggest that the thermal treatment at the time of ion implantation can achieve a thermal treatment effect at a lower temperature than the annealing after the implantation. Cross-sectional high-angle annular dark field STEM imaging and energy dispersive X-ray spectroscopy (EDS) were carried out to confirm whether Mg accumulated at the elliptical defects in the 1000 °C implantation sample after post-implantation annealing. However, we were unable to confirm the Mg accumulation at the defects. The detection limit of EDS was about 1×10^{21} cm^{-3} in the case of uniform

distribution, and it has been clarified that there is no segregation of high-concentration Mg at the defects. From the number of defects generated by Mg ion implantation, it appears that, among all Mg-ion-implanted GaN samples [Figs. 5 and 7], the number of defects in the 1000 °C implantation sample after annealing is the smallest [Fig. 7(c)], and that the crystallinity recovered in most of the areas other than the defects. It can be seen that the crystallinity after annealing varies greatly with the implantation temperature, and it seems that Mg ion implantation at 1000 °C can greatly improve the crystallinity after Mg ion implantation. In addition, this result suggests that the recovery after post-implantation annealing is promoted by maintaining good crystallinity before post-implantation annealing. It also suggests that recovery after post-implantation annealing is difficult after crystallinity is destroyed by RT implantation. On the other hand, as compared with the as-implanted samples, the after annealing samples shows crystal distortion near the GaN surface. These results are thought to be due to the post-implantation annealing performed at a temperature higher than the implantation temperature, resulting in distortion due to N out-diffusion from GaN surface or due to differences in thermal expansion between SiN and GaN.

Vertical diodes were fabricated and evaluated using the Mg-ion-implanted GaN samples after annealing. Figure 8 shows the current−voltage (I−V) characteristics of vertical diodes fabricated using Mg-ion-implanted GaN. In the RT implantation sample [Fig. 8(a)], the reverse leakage current was large and no clear rectification was observed. Compared with the RT implantation sample, the reverse current was lower in the 800 °C implantation sample [Fig. 8(b)]. In addition, in the 1000 °C implantation sample [Fig. 8(c)], the reverse current was lower than that in the 800 °C implantation sample and the forward on-voltage was improved. Also, the on-resistance of the 1000 °C implantation sample was reduced to less than half compared with that of the RT implantation sample. But electroluminescence emission was not observed. The forward on-voltage was about 4 to 5 V, which is higher than that of epitaxially grown p−n diodes,[29] which is about 3 V as expected from the built-in potential. It has been reported that this phenomenon occurs in Mg-ion-implanted GaN vertical diode, and is attributed to incomplete ohmic contact.[12,30] This result is probably due to the fact that an ohmic contact is not achieved because acceptor compensation occurs due to V_Ns or other causes, and the activation ratio of the implanted Mg is not high. However, the Mg-ion-implanted layer of the 1000 °C implantation sample is considered to have the

following characteristics. At a small reverse leakage current, implanted Mg acts as an acceptor ion that forms a depletion layer at the time of reverse bias, at a decreased on-resistance, they are considered to function as supply holes at the time of forward bias. On the basis of these results, the *I*–*V* characteristics of Mg-ion-implanted GaN vertical diodes in this study suggest that Mg was activated. In addition, these results are considered to be consistent with the fact that the higher the implantation temperature in the PL spectra of the samples after annealing, the higher the intensity of the DAP emission, suggesting improved Mg activation.

In GaN annealed by implanting with Mg ions at 1000 °C, the NBE emission intensity in the low-temperature PL measurement was higher than that in the other samples, suggesting a decrease of the concentration of nonradiative recombination channels, and the greatest amount of crystallinity recovery was observed in the cross-sectional TEM image. Furthermore, from the *I*–*V* characteristics, a forward on-voltage, indicating Mg activation, was confirmed. These results indicate that high-temperature implantation of Mg ions into GaN improves the crystallinity and helps activate Mg after ion implantation compared with RT implantation.

4. Conclusions

We performed Mg ion implantation into GaN at high temperatures and investigated the most appropriate temperature for Mg ion implantation into GaN. A GaN sample that was implanted with Mg ions at 1000 °C then and post-implantation annealed at 1250 °C for 20 s showed the following characteristics. In the low-temperature PL measurement, an increase in NBE emission intensity was observed, suggesting a decrease of the concentration of nonradiative recombination channels, and from the cross-sectional TEM image, it was confirmed that the number of defects generated by Mg ion implantation decreased and the crystallinity recovered significantly. The on-voltage *I*–*V* characteristics of the Mg-ion-implanted GaN vertical diodes indicated Mg activation, and clear rectifying properties were observed. Therefore, high-temperature implantation of Mg ions into GaN was confirmed to be useful, and these results suggest that implantation at 1000 °C or higher was necessary to obtain the high-temperature implantation effect.

Acknowledgments

This work was supported by the Cross-ministerial Strategic Innovation Promotion Program (SIP) and MEXT “Program for research and development of next-generation semiconductor to realize energy-saving society”. The authors would like to thank Professor Akira Uedono (Tsukuba University) and Professor Tohru Nakamura (Hosei University) for useful discussions.

References

1) A. Uedono, S. Takashima, M. Edo, K. Ueno, H. Matsuyama, W. Egger, T. Koschine, C. Hugenschmidt, M. Dickmann, K. Kojima, S. F. Chichibu, and S. Ishibashi, Phys. Status Solidi B **255**, 1700521 (2018).
2) S. F. Chichibu, K. Shima, K. Kojima, S. Takashima, K. Ueno, M. Edo, H. Iguchi, T. Narita, K. Kataoka, S. Ishibashi, and A. Uedono, Jpn. J. Appl. Phys. **58**, SC0802 (2019).
3) C. G. Van de Walle and J. Neugebauer, J. Appl. Phys. **95**, 3851 (2004).
4) A. Uedono, S. Takashima, M. Edo, K. Ueno, H. Matsuyama, H. Kudo, H. Naramoto, and S. Ishibashi, Phys. Status Solidi B **252**, 2794 (2015).
5) A. Wenzel, C. Liu, and B. Rauschenbach, Mater. Sci. Eng. B **59**, 191 (1999).
6) S. Whelan, M. J. Kelly, R. Gwilliam, C. Jeynes, and C. Bongiorno, J. Appl. Phys. **98**, 013515 (2005).
7) A. Lardeau-Falcy, M. Coig, M. Charles, C. Licitra, J. Kanyandekwe, F. Milési, J. Eymery, and F. Mazen, ECS Trans. **80**, 131 (2017).
8) T. Niwa, T. Fujii, and T. Oka, Appl. Phys. Express **10**, 091002 (2017).
9) A. Kumar, K. Mitsuishi, T. Hara, K. Kimoto, Y. Irokawa, T. Nabatame, S. Takashima, K. Ueno, M. Edo, and Y. Koide, Nanoscale Res. Lett. **13**, 403 (2018).
10) M. Sumiya, K. Fukuda, S. Takashima, S. Ueda, T. Onuma, T. Yamaguchi, T. Honda, A. Uedono, Journal of Crystal Growth **511**, 15 (2019).
11) I. O. Usov, N. R. Parikh, D. Thomson, and R. F. Davis, Mater. Res. Soc. Symp. Proc. **693**, I11.12 (2001).
12) T. Oikawa, Y. Saijo, S. Kato, T. Mishima, and T. Nakamura, Nucl. Instrum. Methods Phys. Res., Sect. B **365**, 168 (2015).
13) J. D. Greenlee, T. J. Anderson, B. N. Feigelson, K. D. Hobart, and F. J. Kub, Phys. Status Solidi A **212**, 2772 (2015).
14) T. Narita, T. Kachi, K. Kataoka, and T. Uesugi, Appl. Phys. Express **10**, 016501 (2017).
15) R. Tanaka, S. Takashima, K. Ueno, H. Matsuyama, M. Edo, and K. Nakagawa, Appl. Phys. Express **12**, 054001 (2019).
16) M. Yoshino, K. Sugamata, K. Ikeda, T. Nishimura, K. Kuriyama, and T.

Nakamura, Nucl. Instrum. Methods Phys. Res., Sect. B **449**, 49 (2019).

17) M. Yoshino, Y. Ando, M. Deki, T. Toyabe, K. Kuriyama,Y. Honda, T. Nishimura, H. Amano, T. Kachi, and T. Nakamura, Materials **12**, 689 (2019).

18) R. Tanaka, S. Takashima, K. Ueno, H. Matsuyama, and M. Edo, Jpn. J. Appl. Phys. **59**, SGGD02 (2020).

19) H. Sakurai, M. Omori, S. Yamada, Y. Furukawa, H. Suzuki, T. Narita, K. Kataoka, M. Horita, M. Bockowski, J. Suda, and T. Kachi, Appl. Phys. Lett. **115**, 142104 (2019).

20) M. Sumiya, K. Fukuda, H. Iwai, T. Yamaguchi, T. Onuma, and T. Honda, AIP Adv. **8**, 115225 (2018).

21) S. M. C. Miranda, P. Kessler, J. G. Correia, R. Vianden, K. Johnston, E. Alves, and K. Lorenz, Phys. Status Solidi C **9**, 1060 (2012).

22) S. M. C. Miranda, P. R. Edwards, K. P. O'Donnell, M. Boćkowski, E. Alves, I. S. Roqan, A. Vantomme, and K. Lorenz, Phys. Status Solidi C **11**, 253 (2014).

23) M. A. Reshchikov, D. O. Demchenko, J. D. McNamara, S. Fernández-Garrido, and R. Calarco, Phys. Rev. B **90**, 035207 (2014).

24) K. Kojima, S. Takashima, A. Edo, K. Ueno, M. Shimizu, T. Takahashi, S. Ishibashi, A. Uedono, and S. F. Chichibu, Appl. Phys. Express **10**, 061002 (2017).

25) K. Shima, H. Iguchi, T. Narita, K. Kataoka, K. Kojima, A. Uedono, and S. F. Chichibu, Appl. Phys. Lett. **113**, 191901 (2018).

26) A. G. Jacobs, B. N. Feigelson, J. K. Hite, C. A. Gorsak, L. E. Luna, T. J. Anderson, and F. J. Kub, Jpn. J. Appl. Phys. **58**, SCCD07 (2019).

27) S. F. Chichibu, K. Shima, K. Kojima, S. Takashima, M. Edo, K. Ueno, S. Ishibashi, and A. Uedono, Appl. Phys. Lett. **112**, 211901 (2018).

28) A. Kumar, J. Uzuhashi, T. Ohkubo, R. Tanaka, S. Takashima, M. Edo, and K. Hono, J. Appl. Phys. **126**, 235704 (2019).

29) H. Fukushima, S. Usami, M. Ogura, Y. Ando, A. Tanaka, M. Deki, M. Kushimoto, S. Nitta, Y. Honda, and H. Amano, Jpn. J. Appl. Phys. **58**, SCCD25 (2019).

30) T. Nakamura, M. Yoshino, H. Tsuge, K. Ikeda, and K. Kuriyama, Surface & Coatings Technology **355**, 7 (2018).

Figure Captions

Fig. 1. Illustration of simple process flow and Mg-ion-implanted (Mg-I/I) GaN sample structure.

Fig. 2. [Mg] profile obtained by SRIM calculation.

Fig. 3. XRD spectra in $2\theta-\omega$ scan mode of Mg-implanted GaN samples (as-implanted) and unimplanted UID-GaN.

Fig. 4. PL spectra at 77 K for (a) Mg-implanted GaN at RT (as-implanted), (b) Mg-implanted GaN at 800 °C (as-implanted), and (c) Mg-implanted GaN at 1000 °C (as-implanted).

Fig. 5. Cross-sectional TEM images of (a) Mg-implanted GaN at RT (as-implanted), (b) Mg-implanted GaN at 800 °C (as-implanted), and (c) Mg-implanted GaN at 1000 °C (as-implanted).

Fig. 6. PL spectra at 77 K for (a) Mg-implanted GaN at RT (after annealing), (b) Mg-implanted GaN at 800 °C (after annealing), and (c) Mg-implanted GaN at 1000 °C (after annealing). (d) is spectra of NBE and DAP emission regions of (a)−(c) showing the PL intensity axis on a linear scale.

Fig. 7. Cross-sectional TEM images of (a) Mg-implanted GaN at RT (after annealing), (b) Mg-implanted GaN at 800 °C (after annealing), and (c) Mg-implanted GaN at 1000 °C (after annealing).

Fig. 8. $I-V$ characteristics of vertical diodes fabricated using (a) Mg-implanted GaN at RT (after annealing), (b) Mg-implanted GaN at 800 °C (after annealing), and (c) Mg-implanted GaN at 1000 °C (after annealing). The upper row is a semi-log scale and the lower row is a linear scale.

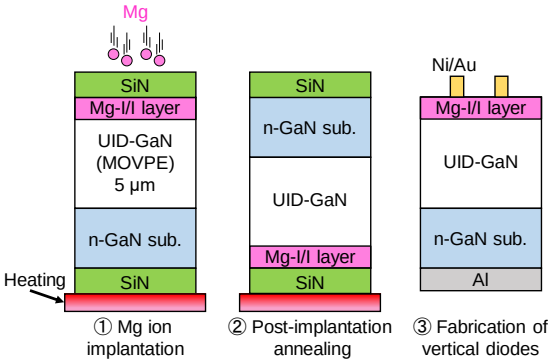
Mg
SiN
Mg-I/I layer
UID-GaN
(MOVPE)
5 μm
n-GaN sub.
SiN
Heating
① Mg ion implantation
SiN
n-GaN sub.
UID-GaN
Mg-I/I layer
SiN
② Post-implantation annealing
Ni/Au
Mg-I/I layer
UID-GaN
n-GaN sub.
Al
③ Fabrication of vertical diodes

Fig. 1.

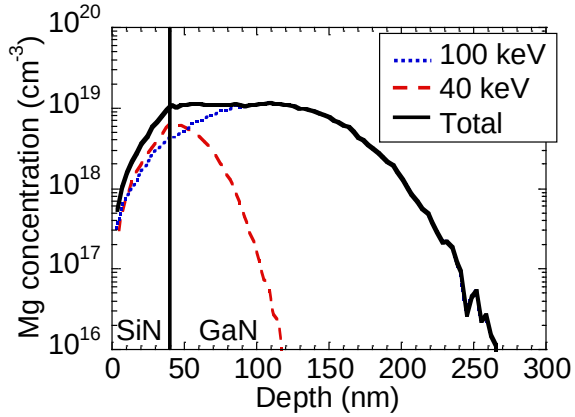
Mg concentration (cm-3)
10^20
10^19
10^18
10^17
10^16
100 keV
40 keV
Total
SiN
GaN
0
50
100
150
200
250
300
Depth (nm)

Fig. 2.

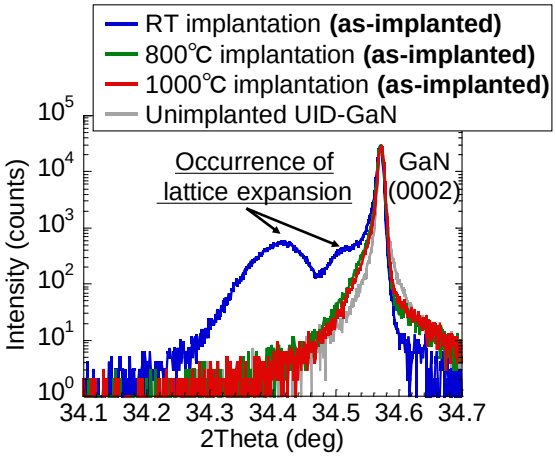
RT implantation (as-implanted)
800℃ implantation (as-implanted)
1000℃ implantation (as-implanted)
Unimplanted UID-GaN
Occurrence of lattice expansion
GaN (0002)
Intensity (counts)
2Theta (deg)

Fig. 3.

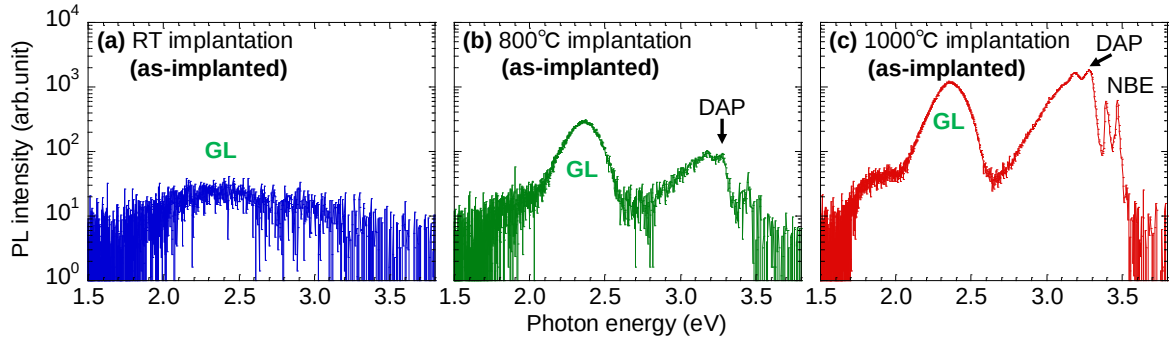
(a) RT implantation
(as-implanted)
GL
(b) 800℃ implantation
(as-implanted)
GL
DAP
(c) 1000℃ implantation
(as-implanted)
GL
DAP
NBE
PL intensity (arb.unit)
Photon energy (eV)

Fig. 4.

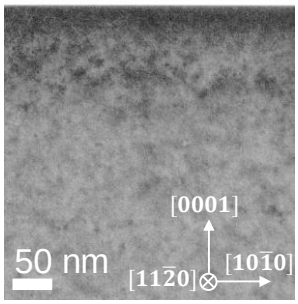

(a) RT implantation **(as-implanted)**

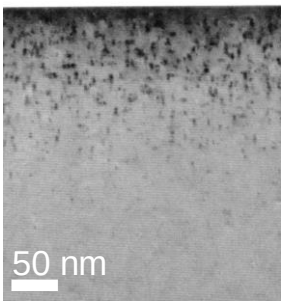

(b) 800℃ implantation **(as-implanted)**

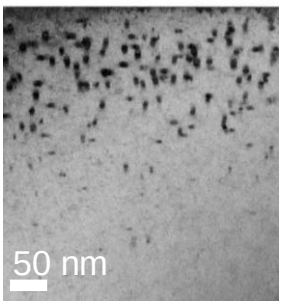

(c) 1000℃ implantation **(as-implanted)**

Fig. 5.

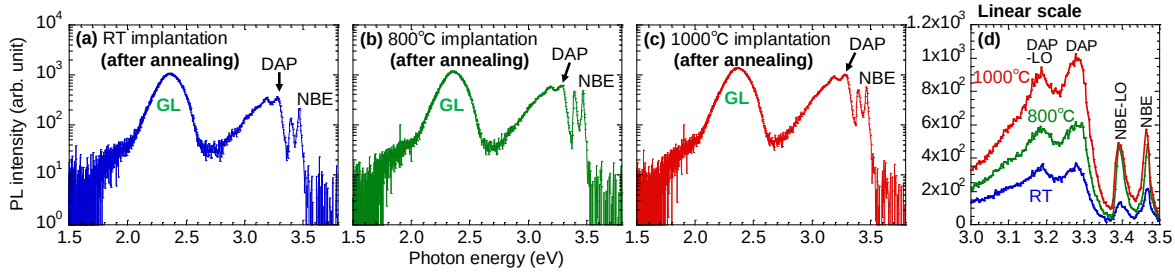
(a) RT implantation
(after annealing)
DAP
NBE
GL
(b) 800℃ implantation
(after annealing)
DAP
NBE
GL
(c) 1000℃ implantation
(after annealing)
DAP
NBE
GL
PL intensity (arb. unit)
Photon energy (eV)
Linear scale
(d)
DAP -LO
DAP
1000℃
800℃
RT
NBE-LO
NBE

Fig. 6.

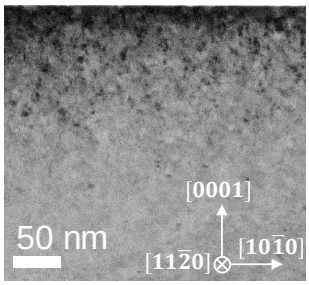

(a) RT implantation **(after annealing)**

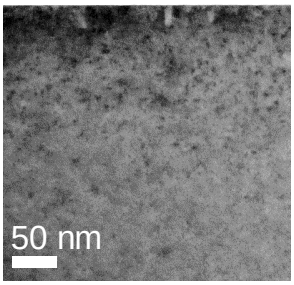

(b) 800℃ implantation **(after annealing)**

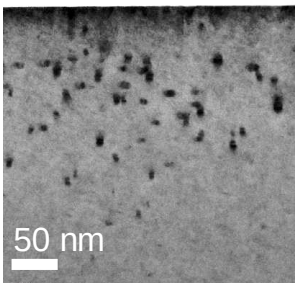

(c) 1000℃ implantation **(after annealing)**

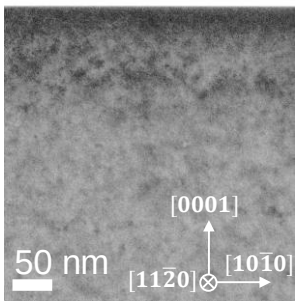

(a) RT implantation **(as-implanted)**

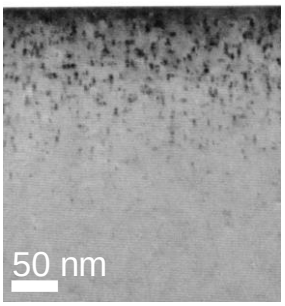

(b) 800℃ implantation **(as-implanted)**

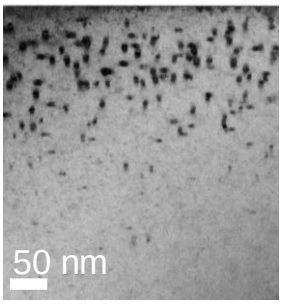

(c) 1000℃ implantation **(as-implanted)**

Fig. 7.

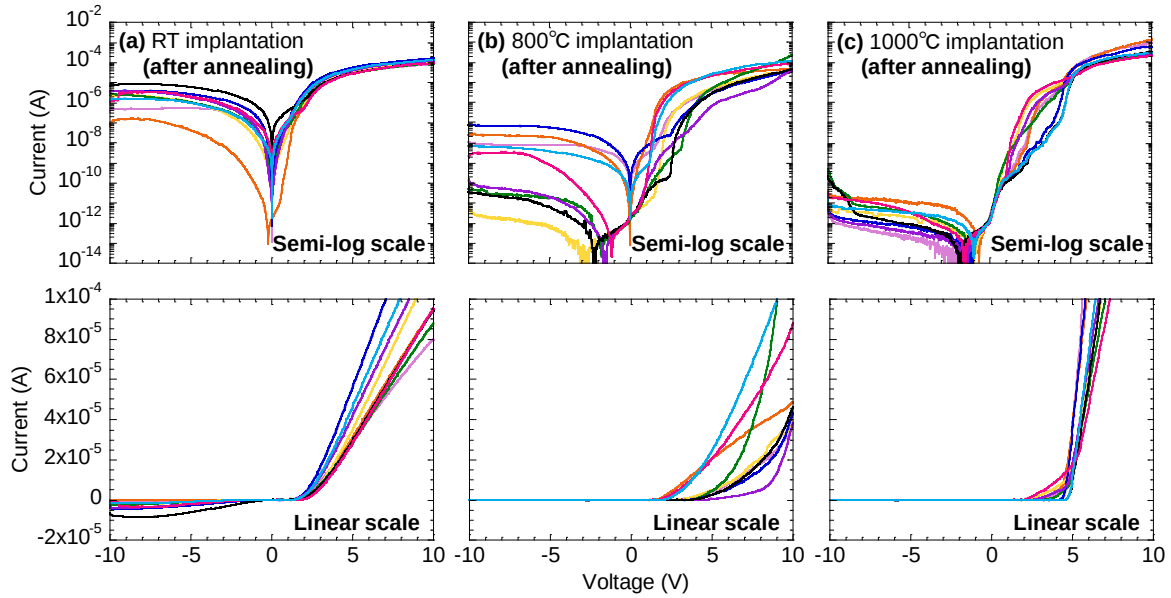
(a) RT implantation
(after annealing)
(b) 800℃ implantation
(after annealing)
(c) 1000℃ implantation
(after annealing)
Semi-log scale
Linear scale
Current (A)
Voltage (V)

Fig. 8.